Supplementary Information

A Fluorinated Zirconium Metal-Organic Cage-Based Supramolecular Framework for Efficient Separation of Methanol-to-Olefins (MTO) Products

Tao Yang[‡a], Zhiyuan Fan[‡a], Jingyang Zheng[‡a], Meng Zhang[a], Tao Chen[a], Yuqing Zhou[a], Changjiang Li*[a], Yao Jiang*[b], and Lin-Bing Sun*[c]

[a] *Key Laboratory of Functional Membranes and Energy Materials and Huangshan Technology Innovation Center for Green Chemical Engineering and New Materials, College of Chemistry and Chemical Engineering, Huangshan University, Huangshan 245041, China;*

[b] *School of Chemistry and Chemical Engineering, Hefei University of Technology, Hefei 230009, China;*

[c] *State Key Laboratory of Materials-Oriented Chemical Engineering, Jiangsu National Synergetic Innovation Center for Advanced Material (SICAM), College of Chemical Engineering, Nanjing Tech University, Nanjing 211816, China.*

**Corresponding author. E-mail: 163licj@163.com; yjiang@hfut.edu.cn; lbsun@njtech.edu.cn.*

Experimental Details

Chemicals

Bis(cyclopentadienyl)zirconium dichloride (Cp_2ZrCl_2; Aldrich, 98%), tetrafluoroterephthalic acid (Adamas, 98%), *N, N*-dimethylacetamide (DMA; Aldrich, 99.5 %), dichloromethane (DCM; Aldrich, 99.5%), and dimethyl sulfoxide-d_6 (DMSO-d_6; Adamas, 99.9%) were purchased from suppliers and used directly without any further purification. Deionized water was generated by a Milli-Q integral pure and ultrapure water purification system and used in all experiments.

Materials synthesis

Synthesis of NUT-107

15 mg zirconocene dichloride and 5 mg tetrafluoroterephthalic acid were dissolved in 1 mL DMA in a glass vial by ultrasonic treatment and 150 μL deionized water was added to the mixture, which was placed in an oven preheated to 60 °C for 4 h. After cooling, NUT-107 was collected as a white crystal, and after washing with DMA and DCM three times for further use.

Characterization

Single crystals of NUT-107 were selected on a Bruker D8 VENTURE MetalJet PHOTON II diffractometer. The crystal was kept at 193.00 K during data collection. The structure was solved by direct methods and refined by full-matrix least-squares on F^2 with anisotropic displacement using the SHELXTL software package.[1] Non-hydrogen atoms were refined with anisotropic displacement parameters during the final refinement cycles. Hydrogen atoms were placed in calculated positions with isotropic displacement parameters set to 1.2 × U_{eq} of the attached atom. The content of the voids was partially recognizable as DMA and H_2O molecules, but mostly highly disordered. Attempts to include solvent molecules in the structural model yielded less than satisfactory results. The data were thus instead corrected for the contribution of the solvate molecules to the electron density using back Fourier transform methods as implemented in the Squeeze algorithm of the Platon program package.[2] The details for

data collection and refinement are included in the CIF file in the Tables S1-S3. CCDC 2524019 contains the supplementary crystallographic data for this paper. These data can be obtained free of charge from the Cambridge Crystallographic Data Centre (https://www.ccdc.cam.ac.uk/). Powder X-ray diffraction (PXRD) patterns of the materials were recorded with an X-ray diffractometer (Japan Rigaku D/MAX-γA) using Cu Kα radiation at 40 kV and 100 mA. High-resolution mass spectrometry (HR-MS) analysis was performed using a Thermo Scientific Q Exactive hybrid quadrupole-Orbitrap mass spectrometer from the United States. Scanning electron microscopy (SEM), corresponding elemental mapping analysis, and energy-dispersive X-ray spectroscopy (EDS) analysis were performed using a Hitachi TM 3000 electron microscope operated at 2 kV. ^{1}H nuclear magnetic resonance (NMR) spectra were recorded on a Bruker AVANCE-400 MHz instrument. Fourier transform infrared (FT-IR) spectra of the samples diluted with KBr were carried out on a ThermoFisher Nicolet iS10 spectrometer. X-ray photoelectron spectroscopy (XPS) was tested through a Thermo Scientific ESCALAB 250Xi spectrometer. The thermogravimetric analysis (TGA) curve was obtained by use of a thermobalance (STA-499C, NETZSCH). The sample was heated from room temperature to 800 ^{o}C with the heating rate 10 ^{o}C·min^{-1} under a flow of N_2 (10 mL·min^{-1}).

Adsorption tests

C_3H_6 and C_2H_4 adsorption isotherms were collected on an ASAP 2020 analyzer. Before each measurement, the sample was degassed under a vacuum line of ASAP 2020 at 353 K for 4 h to completely remove the guest molecules in the pores of NUT-107 to be tested. Ultra-high purity grades C_3H_6 (99.99%) and C_2H_4 (99.99%) were used for gas adsorption measurements. The N_2 adsorption-desorption isotherms were measured at 77 K using the automatic multi-station-specific surface, micropore, and mesoporous pore analyzer belcorp-max of Microtracbel Company. The samples were degassed at 353 K for 4 h before analysis. The Brunauer-Emmett-Teller (BET) surface area was calculated using adsorption data in a relative pressure ranging from 0.01 to 0.10. The total pore volume was determined from the amount adsorbed at a relative pressure of

0.99. The pore diameter was calculated from the adsorption branch using the non-local density functional theory method. To investigate the adsorption selectivity of C_3H_6 and C_2H_4 on the sample of NUT-107, the selectivity is defined as:

$$S = \frac{x_1 / y_1}{x_2 / y_2}$$

where x_1 and y_1 (x_2 and y_2) are the molar fractions of component 1 (component 2) in the adsorbed and bulk phases, respectively. The ideal adsorption solution theory (IAST) of Myers has been reported to predict binary gas mixture adsorption in porous materials accurately,[3] and the single-site Langmuir-Freundlich equation (LF) model was chosen to fit the adsorption isotherms, and then IAST was utilized to estimate the C_3H_6 and C_2H_4 selectivity of the adsorbent.

Calculation of heat of adsorption (Q_{st})

The Q_{st} is based on the adsorption isotherm data of the adsorbent on the gas at different temperatures. According to the Virial equation:

$$\ln P = \ln N + (\frac{1}{T})\sum_{i=0}^{m} a_i \times N^i + \sum_{j=0}^{n} b_j \times N^j$$

$$Q_{st} = -R \times \sum_{i=0}^{m} a_i \times N^i$$

Where P is the pressure (kPa); N is the adsorption amount (mmol·g^{-1}); T is the adsorption temperature; R is ideal gas constant (8.314 J·mol^{-1}·K^{-1}); m and n are the number of a and b parameters, respectively.

Separation potential

The separation effect of different adsorbents can be evaluated by comparing the separation potential directly.[4, 5]

$$\Delta q = q_{C_3H_6}\frac{y_{C_2H_4}}{y_{C_3H_6}} - q_{C_2H_4}$$

where $q_{C_3H_6}$ and $q_{C_2H_4}$ are C_3H_6 and C_2H_4 adsorption in the mixture, respectively. For a 50/50 mixture, formula can be simplified as

$$\Delta q = q_{C_3H_6} - q_{C_2H_4}$$

The physical significance of Δq is that it represents the maximum amount of pure C_3H_6 that can be recovered during the adsorption phase of fixed-bed separation.

Dynamic breakthrough test

The samples after several washes were loaded into quartz tubes of size ø 4 mm × 150 mm and activated in a vacuum oven at 60 °C for 4 hours. He was used as a carrier gas to purge the line, and the C_3H_6/C_2H_4 (50:50, v: v) gas mixtures were flow controlled by a mass flow meter. The flow rate was adjusted to 2.5 mL·min^{-1} during testing. The gas at the outlet of the adsorption column is continuously monitored using a thermal conductivity detector (TCD) and a flame ionization detector (FID).

Methodology

Density functional theory (DFT) calculations were performed to investigate the adsorption behavior of C_2H_4/C_3H_6 molecules on the NUT-107 using the *Quantum ESPRESSO* package.[6, 7] based on the pseudopotential plane-wave (PPW) method. An ultra-soft pseudopotential and a plane wave basis set were used in the GGA-type PBE-D2 functional for the relaxation.[8, 9]. The pseudopotentials for C, H, O, F, Zr, and Cl were taken from the Quantum ESPRESSO pseudopotential library (https://www.quantum-espresso.org/pseudopotentials). All atomic structures were fully relaxed, with all atomic positions allowed to relax during geometry optimizations. Brillouin-zone sampling was performed using Monkhorst-Pack k-point grids with a reciprocal-space spacing of approximately 0.04 Å^{-1}.[10, 11] A kinetic energy cutoff of 50 Ry. As the relaxation proceeded, the atomic positions and lattice vector were simultaneously modified until the residual forces and energy were less than 10^{-4} Ry/Bohrs and 10^{-5} Ry, respectively.

All grand canonical Monte Carlo (GCMC) computations were carried out by the open-source software package RASPA.[12] The Lennard-Jones potential was used with the applied universal force field (UFF) for the NUT-107 adsorbent atoms and with the Transferable Potentials for Phase Equilibria (TraPPE) force field for adsorbate molecule atoms.[13, 14] The Lorentz-Berthelot rule was set to generate the interaction

parameters between NUT-107 and adsorbate molecules, and the cut-off distance was set as 12 Å.[15] Before conducting uptake simulation, NUT-107 was set as a rigid 1×1×1 cell and exported as a charged structure from charge equilibration (Q_{eq}) first. The charged structure was then used to generate the uptake isotherm, isosteric heat at zero coverage (Q_{st}), preferable binding site (minimization) and density plot of adsorption with ethylene (C_2H_4) and propylene (C_3H_6) molecules, respectively. As for the uptake isotherm simulation, the simulated pressure was set to range from 0 bar to 1 bar with an interval of 0.1 bar. For each pressure point, the simulation input was set as 273 K, and a total of 1.0×10^5 cycles Monte Carlo moves were set equally with the probabilities for adsorbate translation, rotation, reinsertion, and swap moves 0.5, 0.5, 0.5 and 1.0. As for the Q_{st} calculation, the simulated pressure was set to 0 bar and only the Monte Carlo moves were set only with the widom-particle insertion.[16] Next for the minimization process, the Baker minimization method was employed using the eigenvalues/vectors to find a true minimum where all eigenvalues are positive.[17] Finally, the density plot and minimization results were plotted via iRASPA.[18] The detailed parameters of the force field for both NUT-107 and molecules are shown in Table S6.

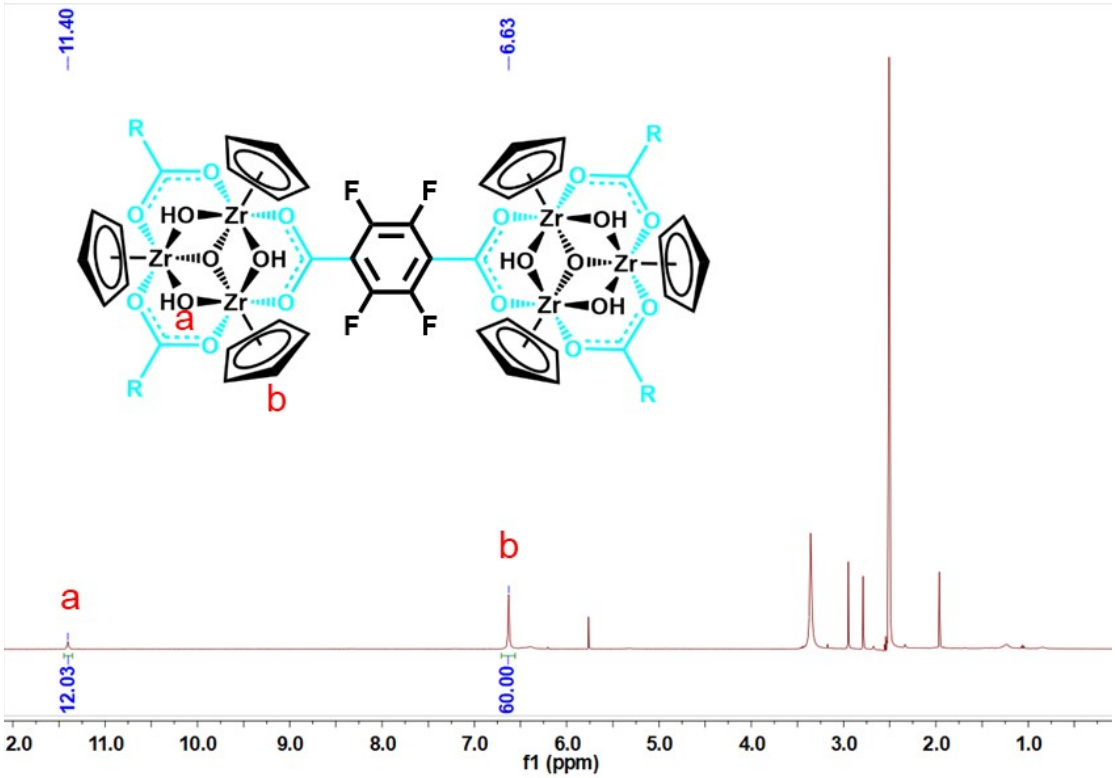

Fig. S1 ^{1}H NMR spectrum of NUT-107 in DMSO-d_6.

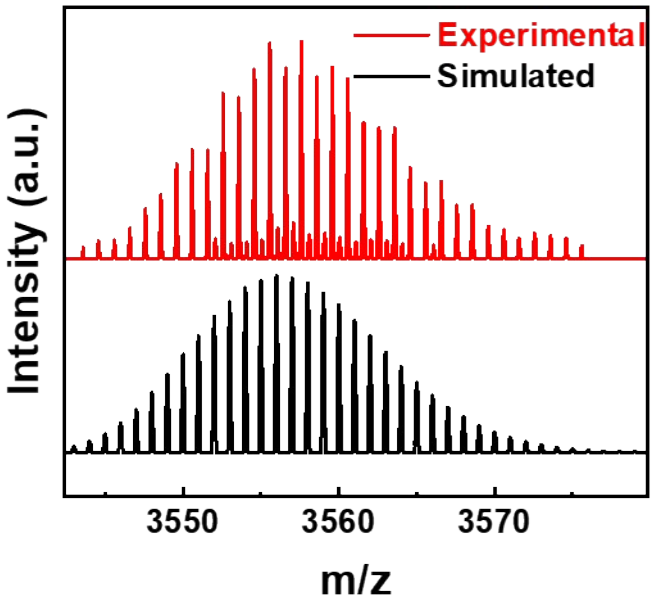

Fig. S2 The experimental and simulated isotope patterns of +1 charge state peaks are attributed to the tetrahedral cage of NUT-107.

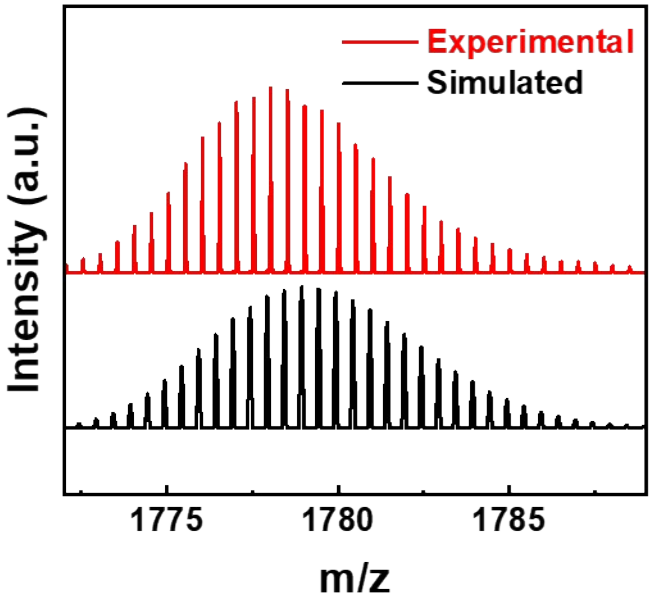

Fig. S3 The experimental and simulated isotope patterns of +2 charge state peaks are attributed to the tetrahedral cage of NUT-107.

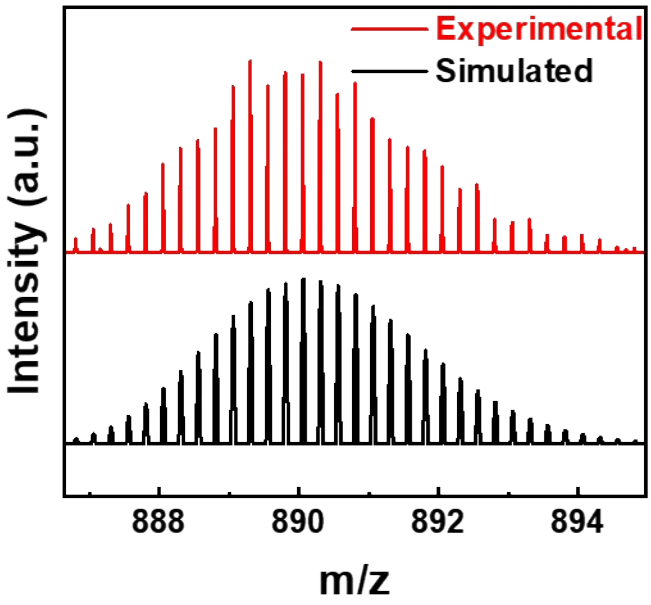

Fig. S4 The experimental and simulated isotope patterns of +4 charge state peaks are attributed to the tetrahedral cage of NUT-107.

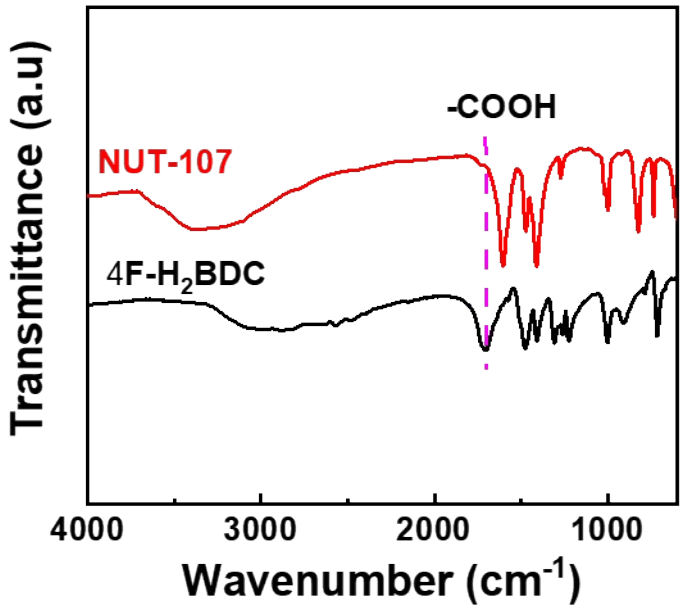

Fig. S5 FT-IR spectra of 4F-H_2BDC and NUT-107.

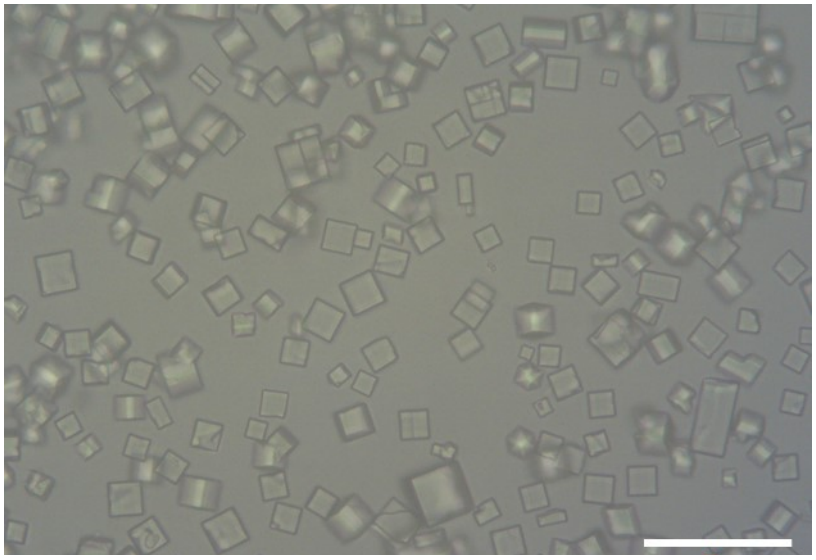

Fig. S6 The optical microscope of the NUT-107 (scale bar 50 μm).

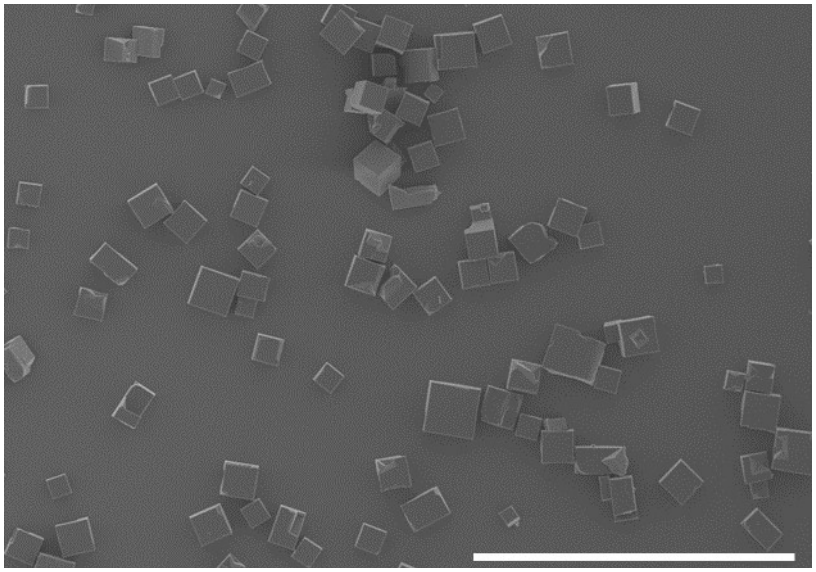

Fig. S7 SEM images of NUT-107.

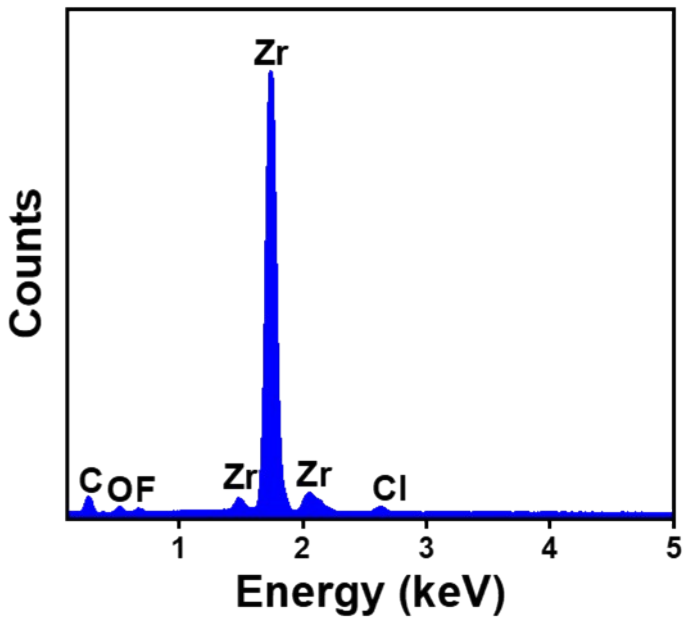

Fig. S8 EDX spectrum of the sample NUT-107.

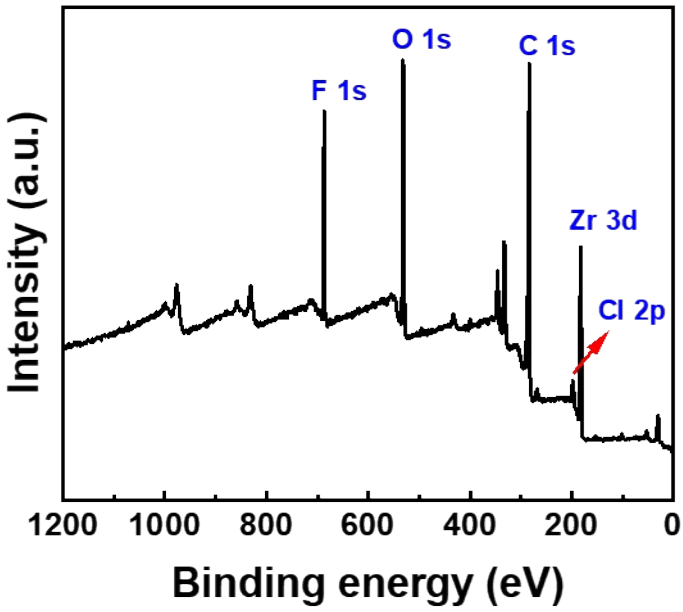

Fig. S9 XPS survey spectrum of NUT-107.

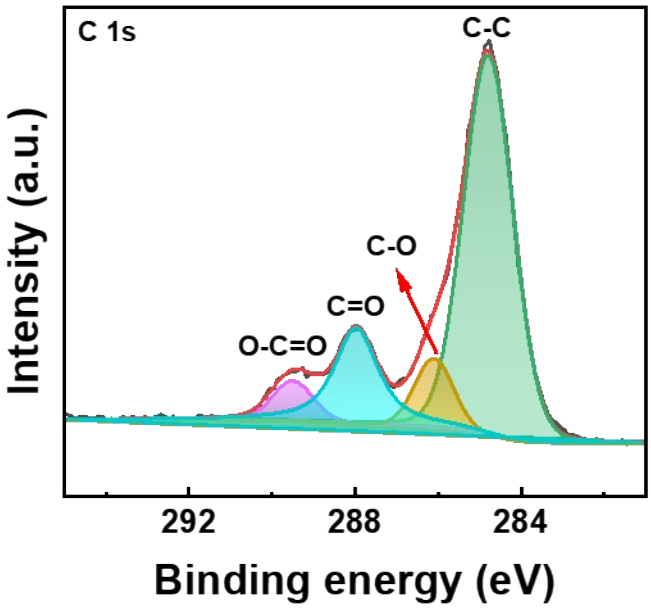

Fig. S10 XPS spectrum of C elements of NUT-107.

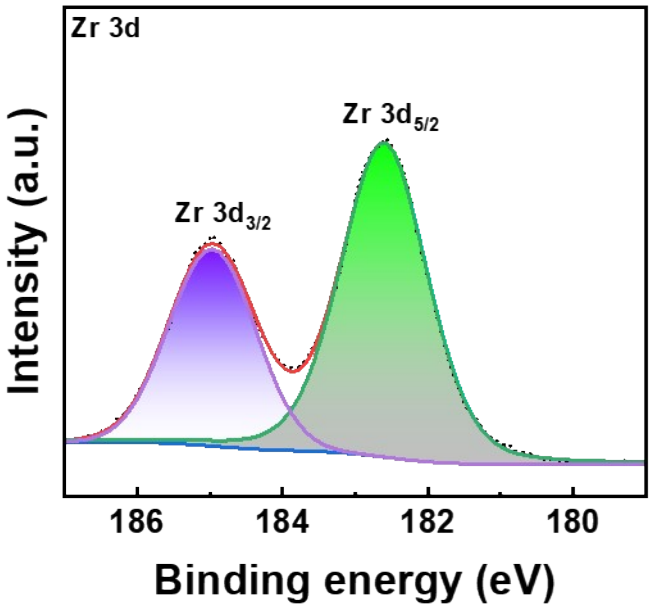

Fig. S11 XPS spectrum of Zr elements of NUT-107.

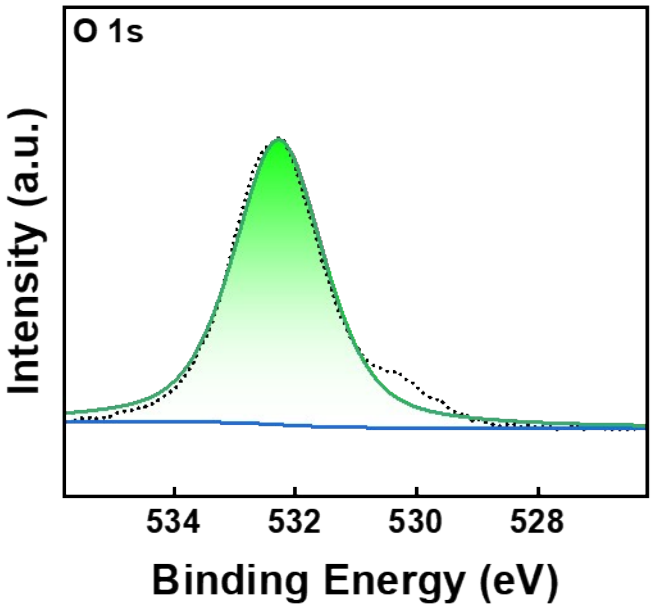

Fig. S12 XPS spectrum of O elements of NUT-107.

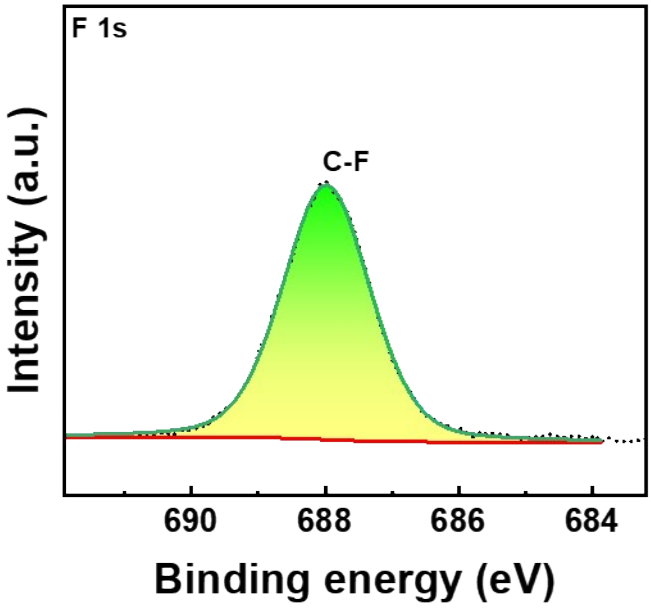

Fig. S13 XPS spectrum of F elements of NUT-107.

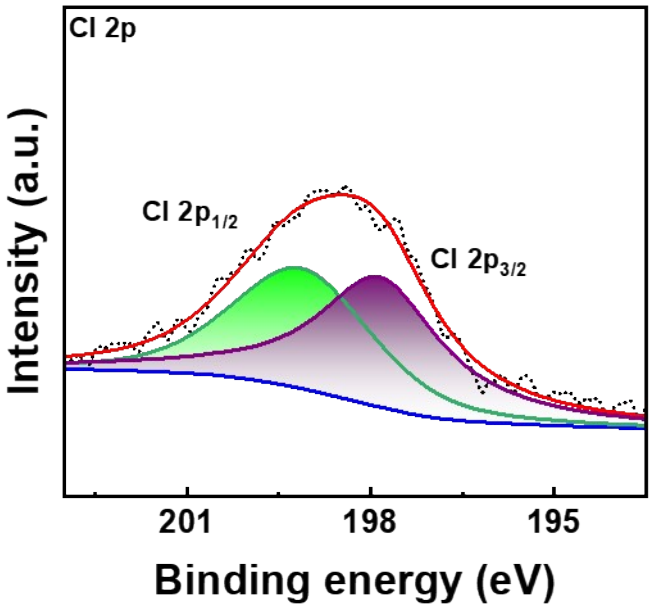

Fig. S14 XPS spectrum of Cl elements of NUT-107.

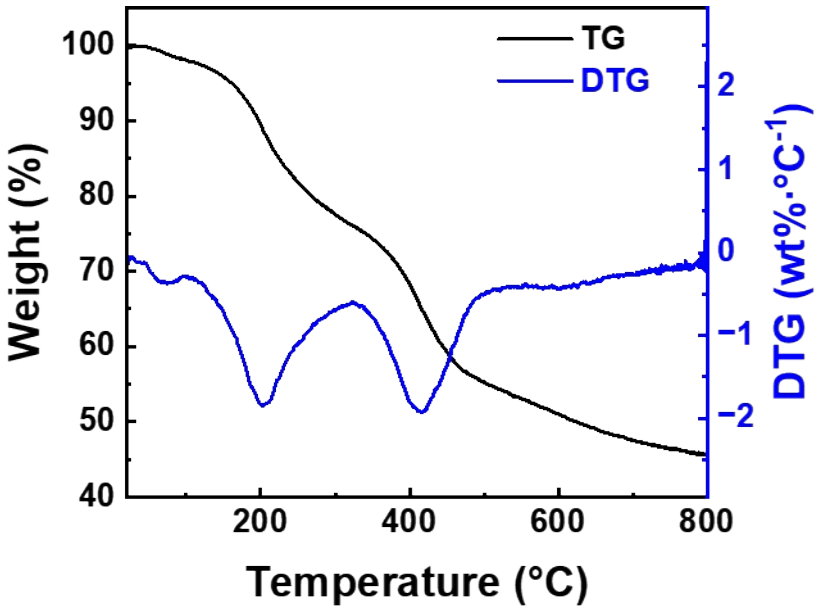

Fig. S15 TGA and DTG curves of the NUT-107.

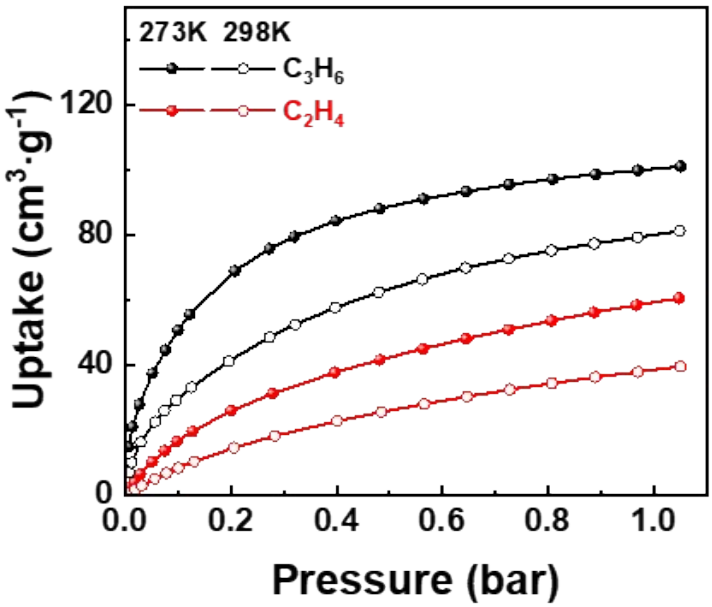

Fig. S16 The uptake for C_3H_6/C_2H_4 at 273/298 K for a non-fluorinated supramolecular framework.

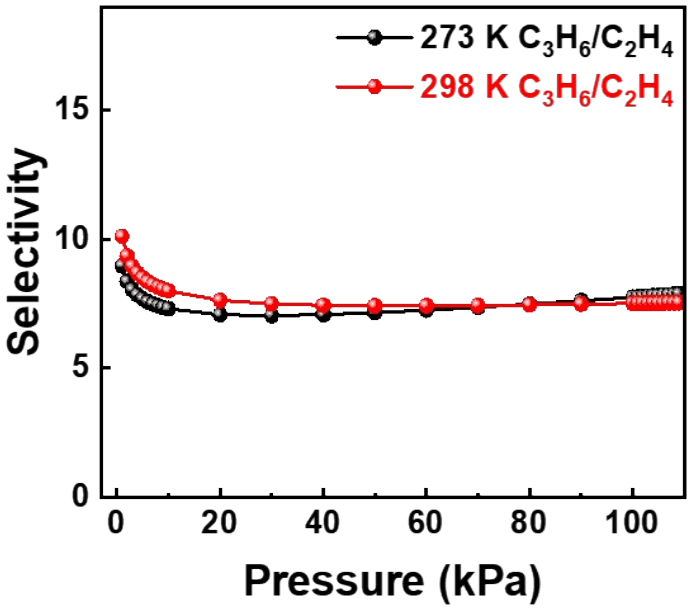

Fig. S17 IAST selectivity for C_3H_6/C_2H_4 at 273 and 298 K for NUT-107.

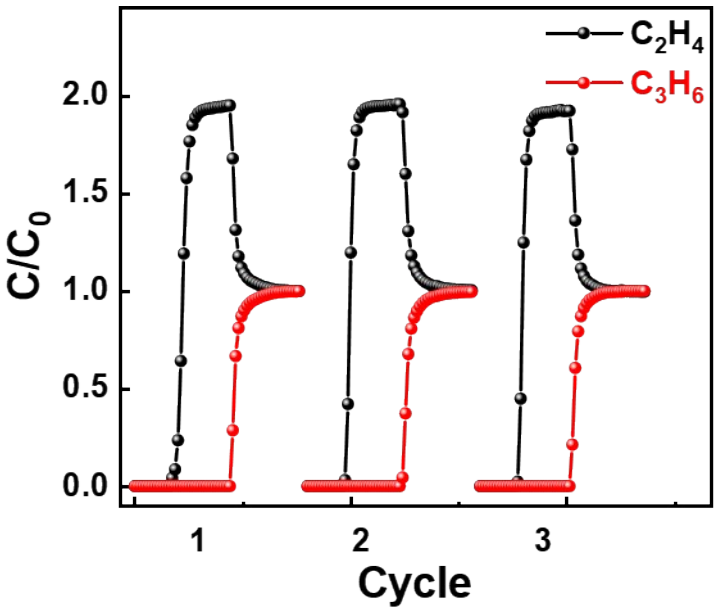

Fig. S18 Breakthrough cycle curves of C_2H_4/C_3H_6 (50:50, v: v) mixtures on NUT-107 at 1.0 bar and 273 K.

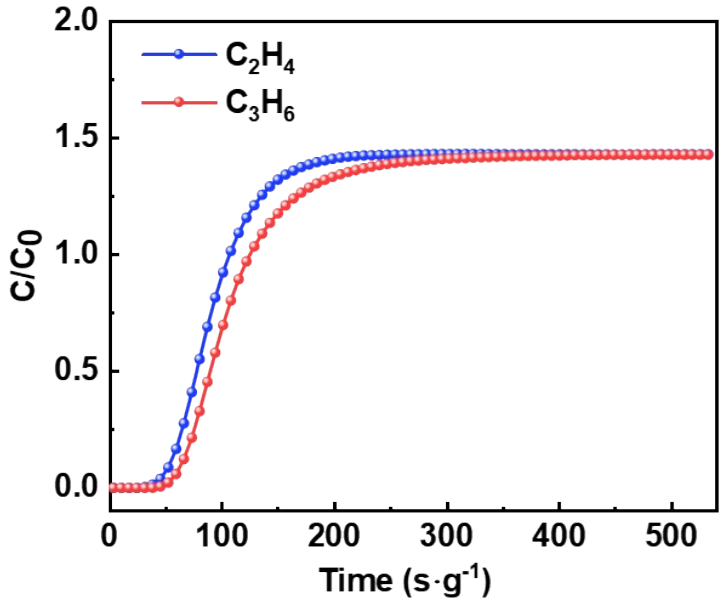

Fig. S19 Breakthrough of C_2H_4/C_3H_6 (50:50, v:v) mixtures on NUT-107 at 40% relative humidity conditions.

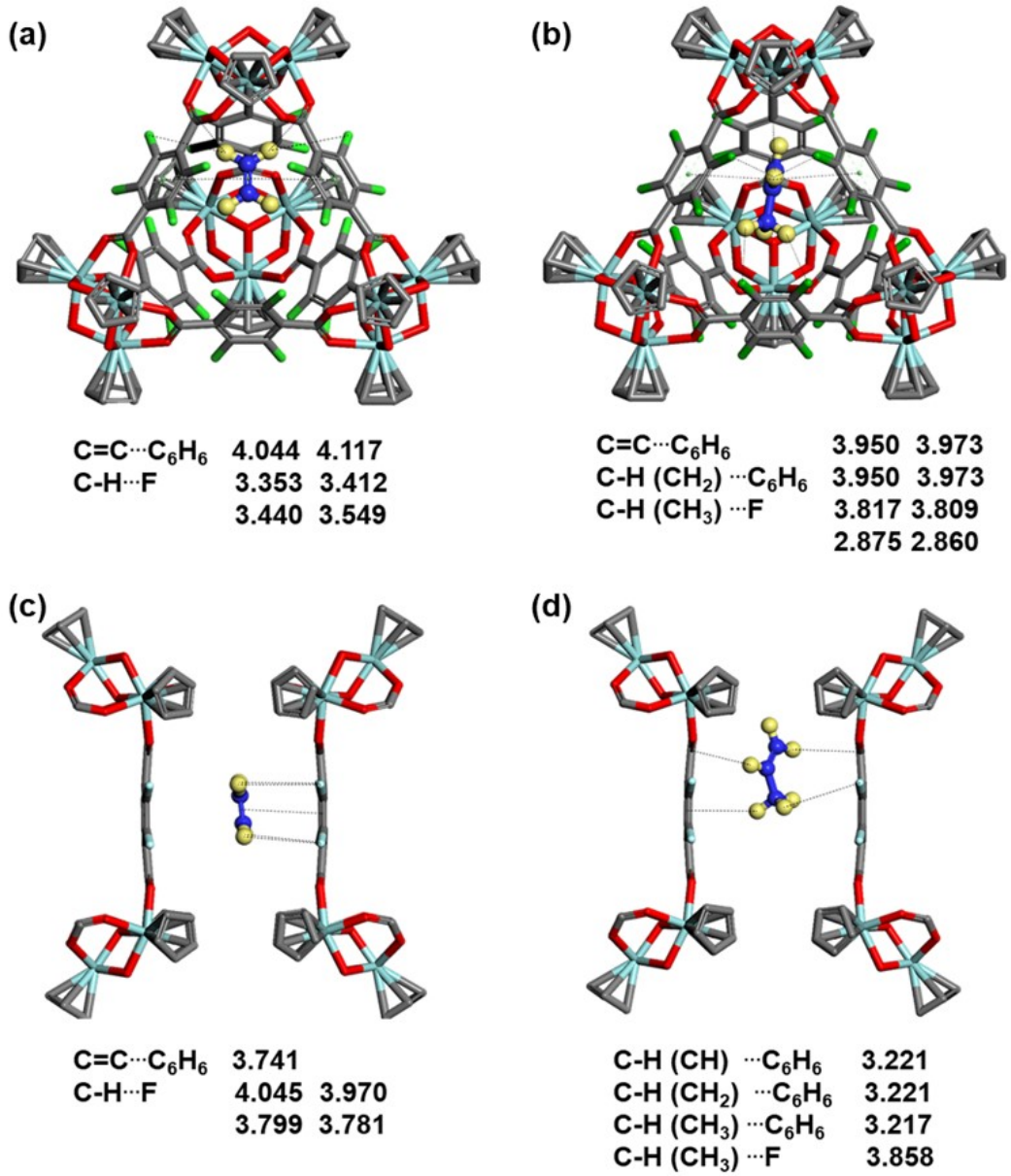

Fig. S20 Adsorption sites for C_2H_4 and C_3H_6 are identified in the inner cage (a-b) and in the interstitial region between adjacent cages (c-d). The interactions of the cage and the gas molecules are depicted by dashed bonds, and the unit of distance is Å.

Table S1. Summary of crystal data and structure refinement parameters of NUT-107.

Compound	NUT-107
CCDC number	2524019
Empirical formula	$C_{108}H_{74}Cl_6F_{24}O_{40}Zr_{12}$·2DMA·$H_2O$
Formula weight	3967.27
Temperature/K	193.00
Crystal system	cubic
Space group	*Fm-3m*
a/Å	37.167(3)
b/Å	37.167(3)
c/Å	37.167(3)
α/°	90
β/°	90
γ/°	90
Volume/Å^3	51342(11)
Z	8
ρcalcg/cm^3	1.027
μ/mm^{-1}	3.302
F(000)	15568.0
Crystal size/mm^3	0.12 × 0.1 × 0.08
Radiation	GaKα (λ = 1.34139)
2θ range for data collection/°	13.592 - 104.042
Index ranges	-43 ≤ h ≤ 43, -43 ≤ k ≤ 43, -43 ≤ l ≤ 43
Reflections collected	126496
Independent reflections	2184 [R_{int}= 0.1188, R_{sigma}= 0.0427]
Data/restraints/parameters	2184/195/180
Goodness-of-fit on F^2	1.082
Final R indexes [I>=2σ (I)]	R_1= 0.1381, wR_2= 0.2331
Final R indexes [all data]	R_1= 0.1602, wR_2= 0.2430
Largest diff. peak/hole/e Å^{-3}	0.52/-0.46

Table S2. Selected bond lengths (Å) for NUT-107.

Atom	Atom	Length/Å	Atom	Atom	Length/Å
Zr1	Zr1[1]	3.337(3)	C9	C10[3]	1.390(11)
Zr1	Zr1[2]	3.337(3)	C11	C11[3]	1.389(14)
Zr1	O6	2.109(7)	C11	C10	1.381(13)
Zr1	O6[1]	2.109(7)	C2	C7	1.3900
Zr1	O1	2.10(6)	C2	C3	1.3900
Zr1	C9	2.53(2)	C7	C6	1.3900
Zr1	C11	2.543(15)	C7	F6	1.387(8)
Zr1	C11[3]	2.543(15)	C6	C5	1.3900
Zr1	C10	2.509(15)	C6	F3	1.386(8)
Zr1	C10[3]	2.509(15)	C5	C4	1.3900
Zr1	O7	2.060(6)	C5	C8	1.496(10)
Zr1	O5	2.060(6)	C4	C3	1.3900
O1	C1	1.250(10)	C4	F2	1.385(8)
C1	C2	1.494(10)	C3	F1	1.384(8)
C1	O2	1.252(10)	O4	C8	1.252(10)
C9	C10	1.390(11)	O3	C8	1.249(10)

Table S3. Selected bond angles (°) for NUT-107.

Atom	Atom	Atom	Angle (°)	Atom	Atom	Atom	Angle (°)
Zr1[1]	Zr1	Zr1[2]	60.0	O7	Zr1	C10	152.2(3)
O6[2]	Zr1	Zr1[1]	86.4(3)	O5	Zr1	Zr1[2]	35.9(2)
O6	Zr1	Zr1[1]	37.7(2)	O5	Zr1	Zr1[1]	35.9(2)
O6[2]	Zr1	Zr1[2]	37.7(2)	O5	Zr1	O6	73.0(4)
O6	Zr1	Zr1[2]	86.4(3)	O5	Zr1	O6[2]	73.0(4)
O6	Zr1	O6[2]	93.5(5)	O5	Zr1	O1	85(2)
O6	Zr1	C9	122.8(3)	O5	Zr1	C9	153.1(6)
O6[2]	Zr1	C9	122.8(3)	O5	Zr1	C11	151.7(5)
O6[2]	Zr1	C11[3]	102.5(4)	O5	Zr1	C11[3]	151.7(5)
O6	Zr1	C11[3]	79.5(4)	O5	Zr1	C10	152.2(3)
O6[2]	Zr1	C11	79.5(4)	O5	Zr1	C10[3]	152.2(3)
O6	Zr1	C11	102.5(4)	Zr1[1]	O6	Zr1	104.6(5)
O6	Zr1	C10	131.7(4)	C1	O1	Zr1	136(5)
O6	Zr1	C10[3]	90.7(4)	O1	C1	C2	130(3)
O6[2]	Zr1	C10	90.7(4)	O1	C1	O2	123.1(14)
O6[2]	Zr1	C10[3]	131.7(4)	O2	C1	C2	107(3)
O1	Zr1	Zr1[2]	79.0(16)	C10[3]	C9	Zr1	73.3(11)
O1	Zr1	Zr1[1]	119(2)	C10	C9	Zr1	73.3(11)
O1	Zr1	O6[2]	86(2)	C10[3]	C9	C10	107.9(8)
O1	Zr1	O6	157(3)	C11[3]	C11	Zr1	74.15(17)
O1	Zr1	C9	75.6(19)	C10	C11	Zr1	72.8(10)
O1	Zr1	C11	100(3)	C10	C11	C11[3]	108.1(4)
O1	Zr1	C11[3]	123(2)	C9	C10	Zr1	74.6(11)
O1	Zr1	C10[3]	106.9(18)	C11	C10	Zr1	75.5(10)
O1	Zr1	C10	71(3)	C11	C10	C9	107.9(6)
C9	Zr1	Zr1[1]	149.43(8)	Zr1[1]	O7	Zr1[2]	108.1(5)
C9	Zr1	Zr1[2]	149.43(8)	Zr1[1]	O7	Zr1	108.2(5)
C9	Zr1	C11	52.5(4)	Zr1[2]	O7	Zr1	108.1(5)
C9	Zr1	C11[3]	52.5(4)	Zr1[1]	O5	Zr1	108.2(5)
C11	Zr1	Zr1[1]	136.9(3)	Zr1[1]	O5	Zr1[2]	108.1(5)
C11[3]	Zr1	Zr1[2]	136.9(3)	Zr1[2]	O5	Zr1	108.1(5)
C11	Zr1	Zr1[2]	117.2(3)	C7	C2	C1	120.9(8)
C11[3]	Zr1	Zr1[1]	117.2(3)	C7	C2	C3	120.0
C11	Zr1	C11[3]	31.7(4)	C3	C2	C1	119.1(8)

C10[3]	Zr1	Zr1[2]	168.6(3)	C6	C7	C2	120.0
C10[3]	Zr1	Zr1[1]	122.2(2)	F6	C7	C2	121.0(7)
C10	Zr1	Zr1[2]	122.2(2)	F6	C7	C6	119.0(7)
C10	Zr1	Zr1[1]	168.6(3)	C7	C6	C5	120.0
C10[3]	Zr1	C9	32.1(3)	F3	C6	C7	119.1(8)
C10	Zr1	C9	32.1(3)	F3	C6	C5	120.9(8)
C10	Zr1	C11	31.7(3)	C6	C5	C8	119.6(8)
C10[3]	Zr1	C11[3]	31.7(3)	C4	C5	C6	120.0
C10	Zr1	C11[3]	52.7(3)	C4	C5	C8	120.4(8)
C10[3]	Zr1	C11	52.7(3)	C5	C4	C3	120.0
C10	Zr1	C10[3]	53.2(5)	F2	C4	C5	121.8(8)
O7	Zr1	Zr1[1]	35.9(2)	F2	C4	C3	118.2(8)
O7	Zr1	Zr1[2]	35.9(2)	C4	C3	C2	120.0
O7	Zr1	O6[2]	73.0(4)	F1	C3	C2	120.8(7)
O7	Zr1	O6	73.0(4)	F1	C3	C4	119.2(7)
O7	Zr1	C9	153.1(6)	O4	C8	C5	113(3)
O7	Zr1	C11	151.7(5)	O3	C8	C5	123(3)
O7	Zr1	C11[3]	151.7(5)	O3	C8	O4	123.3(14)
O7	Zr1	C10[3]	152.2(3)				

Table S4. Compare the separation performance of NUT-107 for C_3H_6/C_2H_4 with that of previously reported materials.

Sample	Selectivity	Separation potential (Δq)	Ref.
MOF-808	3.5	none	[19]
$Cd_2(AzDC)_2(TPT)_2$	1.2	none	[20]
NEM-7-Cu	8.6	2.8	[21]
UPC-33	5.3	2.4	[22]
Zn-BPZ-SA	4.8	1.9	[23]
ZIF-8	5.0	none	[24]
TpDf-COF	6.1	none	[25]
PCP 1	3.6	1.5	[26]
srl-MOF	8.0	0.9	[27]
LIFM-38	6.4	1.4	[28]
Mg-MOF-74	4.7	3.5	[29]
NUT-161	5.5	1.5	[30]
NUT-107	**7.5**	**2.6**	**This work**

Table S5. The simulated isosteric heat of adsorption for NUT-107 adsorption.

Name	Molecule name	Isosteric heat of adsorption ($KJ \cdot mol^{-1}$)
NUT-107	C_2H_4	25.2234637908
	C_3H_6	36.1380675105

Table S6. The parameters of the force field for NUT-107 and Molecules.

Molecules	Pseudo Atom	ε/kb (K)	σ (Å)	reference
C_2H_4	CH2_C2H2	85.000	3.675	[14]
C_3H_6	CH3_C3H6	98.000	3.750	[14]
	CH_C3H6	47.000	3.730	[14]
	CH2_C3H6	85.000	3.675	[14]
NUT-107	C	52.838	3.431	[13]
	H	22.142	2.571	[13]
	O	30.193	3.118	[13]
	Zr	34.720	2.780	[13]
	Cl	114.210	3.520	[13]
	F	25.160	3.000	[13]

References

1. O. V. Dolomanov, Bourhis, L.J., Gildea, R.J, Howard, J.A.K. & Puschmann, H., *J. Appl. Cryst.*, 2009, 339-341.
2. A. Spek, *J. Appl. Crystallogr.*, 2003, **36**, 7-13.
3. A. L. Myers and J. M. Prausnitz, *AIChE J.*, 1965, **11**, 121-127.
4. R. Krishna, *RSC Adv.*, 2017, **7**, 35724-35737.
5. R. Krishna, *ACS Omega*, 2020, **5**, 16987-17004.
6. P. Giannozzi, O. Andreussi, T. Brumme, O. Bunau, M. Buongiorno Nardelli, M. Calandra, R. Car, C. Cavazzoni, D. Ceresoli, M. Cococcioni, N. Colonna, I. Carnimeo, A. Dal Corso, S. de Gironcoli, P. Delugas, R. A. DiStasio, A. Ferretti, A. Floris, G. Fratesi, G. Fugallo, R. Gebauer, U. Gerstmann, F. Giustino, T. Gorni, J. Jia, M. Kawamura, H. Y. Ko, A. Kokalj, E. Küçükbenli, M. Lazzeri, M. Marsili, N. Marzari, F. Mauri, N. L. Nguyen, H. V. Nguyen, A. Otero-de-la-Roza, L. Paulatto, S. Poncé, D. Rocca, R. Sabatini, B. Santra, M. Schlipf, A. P. Seitsonen, A. Smogunov, I. Timrov, T. Thonhauser, P. Umari, N. Vast, X. Wu and S. Baroni, *J. Phys.: Condens. Matter*, 2017, **29**, 465901.
7. P. Giannozzi, S. Baroni, N. Bonini, M. Calandra, R. Car, C. Cavazzoni, D. Ceresoli, G. L. Chiarotti, M. Cococcioni, I. Dabo, A. Dal Corso, S. de Gironcoli, S. Fabris, G. Fratesi, R. Gebauer, U. Gerstmann, C. Gougoussis, A. Kokalj, M. Lazzeri, L. Martin-Samos, N. Marzari, F. Mauri, R. Mazzarello, S. Paolini, A. Pasquarello, L. Paulatto, C. Sbraccia, S. Scandolo, G. Sclauzero, A. P. Seitsonen, A. Smogunov, P. Umari and R. M. Wentzcovitch, *J. Phys.: Condens. Matter*, 2009, **21**, 395502.
8. J. P. Perdew, K. Burke and M. Ernzerhof, *Phys. Rev. Lett.*, 1996, **77**, 3865-3868.
9. S. Grimme, J. Antony, S. Ehrlich and H. Krieg, *J. Chem. Phys.*, 2010, **132**.
10. H. J. Monkhorst and J. D. Pack, *Physical Review B*, 1976, **13**, 5188-5192.
11. P. E. Blöchl, O. Jepsen and O. K. Andersen, *Physical Review B*, 1994, **49**, 16223-16233.
12. D. Dubbeldam, S. Calero, D. E. Ellis and R. Q. Snurr, *Mol. Simul.*, 2016, **42**, 81-101.
13. A. K. Rappe, C. J. Casewit, K. S. Colwell, W. A. Goddard, III and W. M. Skiff, *J. Am. Chem. Soc.*, 1992, **114**, 10024-10035.
14. M. G. Martin and J. I. Siepmann, *J. Phys. Chem. B*, 1998, **102**, 2569-2577.
15. J. Delhommelle and P. MilliÉ, *Mol. Phys.*, 2001, **99**, 619-625.
16. A. Bakhshandeh and Y. Levin, *J. Chem. Phys.*, 2022, **156**.
17. D. Dubbeldam, R. Krishna and R. Q. Snurr, *J. Phys. Chem. C*, 2009, **113**, 19317-19327.
18. D. Dubbeldam, S. Calero and T. J. H. Vlugt, *Mol. Simul.*, 2018, **44**, 653-676.
19. J. Xiao, J. Ma, Z. Zhu, Y. Huang and S. Yuan, *J. Mater. Chem. A*, 2025, **13**, 26431-26440.
20. Y. Zhang, X.-Q. Meng, H.-J. Ding, X. Wang, M.-H. Yu, S.-M. Zhang, Z. Chang and X.-H. Bu, *ACS Appl. Mater. Interfaces*, 2019, **11**, 20995-21003.
21. X. Liu, C. Hao, J. Li, Y. Wang, Y. Hou, X. Li, L. Zhao, H. Zhu and W. Guo, *Inorg. Chem. Front.*, 2018, **5**, 2898-2905.
22. W. Fan, Y. Wang, Q. Zhang, A. Kirchon, Z. Xiao, L. Zhang, F. Dai, R. Wang and

D. Sun, *Chem. Eur. J.*, 2018, **24**, 2137-2143.
23. G.-D. Wang, R. Krishna, Y.-Z. Li, Y.-Y. Ma, L. Hou, Y.-Y. Wang and Z. Zhu, *ACS Mater. Lett.*, 2023, **5**, 1091-1099.
24. W. Su, A. Zhang, Y. Sun, M. Ran and X. Wang, *J. Chem. Eng. Data*, 2017, **62**, 417-421.
25. J. Liu, X. Luo, S. Wang, P. Hao, W. Wei, J. Pan and Y. Peng, *Chem. Commun.*, 2025, **61**, 9492-9495.
26. D. Geng, M. Zhang, X. Hang, W. Xie, Y. Qin, Q. Li, Y. Bi and Z. Zheng, *Dalton Trans.*, 2018, **47**, 9008-9013.
27. H. Fang, B. Zheng, Z.-H. Zhang, H.-X. Li, D.-X. Xue and J. Bai, *Angew. Chem. Int. Ed.*, 2021, **60**, 16521-16528.
28. C.-X. Chen, Z.-W. Wei, Q.-F. Qiu, Y.-Z. Fan, C.-C. Cao, H.-P. Wang, J.-J. Jiang, D. Fenske and C.-Y. Su, *Cryst. Growth Des.*, 2017, **17**, 1476-1479.
29. Z. Bao, S. Alnemrat, L. Yu, I. Vasiliev, Q. Ren, X. Lu and S. Deng, *Langmuir*, 2011, **27**, 13554-13562.
30. G. Liu, F. Li, Z.-J. Diao, H.-D. Li, X. Wu, H.-O. Qi, L. Ding and L.-B. Sun, *J. Mater. Chem. A*, 2025, **13**, 29016-29026.